Analysis of the impedance spectra of short conductive fiber-reinforced composites

by
J. M. Torrents, T. O. Mason
Department of Materials Science and Engineering
Northwestern University
Evanston, IL 60208

A. Peled, S. P. Shah
Department of Civil Engineering
Northwestern University
Evanston, IL 60208

and
E. J. Garboczi
Building and Fire Research Laboratory
National Institute of Standards and Technology
Gaithersburg, MD 20899 USA

Reprinted from Journal of Materials Science, Vol. 36, No. 16, 4003-4012, August 2001.

NIST
National Institute of Standards and Technology
Technology Administration, U.S. Department of Commerce

JOURNAL OF MATERIALS SCIENCE **36** (2001) 4003–4012

Analysis of the impedance spectra of short conductive fiber-reinforced composites

J. M. TORRENTS*, T. O. MASON
Department of Materials Science and Engineering, Northwestern University, Evanston, IL 60208, USA
E-mail: t-mason@northwestern.edu

A. PELED, S. P. SHAH
Department of Civil Engineering, Northwestern University, Evanston, IL 60208, USA

E. J. GARBOCZI
National Institute of Standards and Technology, Building Materials Division, Gaithersburg, MD 20899, USA

The presence of small amounts of short conductive fibers in a composite of finite matrix conductivity results in the subdivision of the one matrix impedance arc into two separate low and high frequency arcs in the complex impedance plane. These features are attributable to a "frequency-switchable" interfacial impedance on the fiber surfaces, rendering them insulating at DC and low AC frequencies, but conducting at intermediate frequencies. A combination of physical simulations (single wires in tap water) and pixel-based computer modeling was employed to investigate the roles of fiber pull-out, debonding, and orientation on the impedance response of fiber-reinforced composites. The ratio of the low frequency arc size to the overall DC resistance (γ-parameter) is sensitive to pull-out and/or debonding, especially when a fiber just barely makes contact with the matrix. The γ-parameter is also quite sensitive to fiber orientation with respect to the direction of the applied field. Ramifications for the characterization of cement, ceramic, and polymer matrix composites are discussed.

1. Introduction

The addition of fibers to an otherwise brittle matrix has a profound influence on the mechanical properties of the composite. By "fiber" is meant an object that is approximately axisymmetric, and much longer than it is wide. The aspect ratio, the ratio of length to width, is usually on the order of 100 or more for typical fibers.

The addition of fibers can also have a strong effect on the electrical properties (DC conductivity and AC impedance) of the composite, but only when the added fibers are highly conductive compared to the matrix [1]. Long, thin inclusions like fibers, which are insulating with respect to the matrix, have little effect on overall electrical properties [1], although of course they can still affect mechanical properties. But if the fibers, which are usually added for mechanical purposes, are highly conducting with respect to the matrix, electrical measurements, which are indirect and non-destructive, are sensitive to the presence of fibers. If the properties of the fibers with respect to the matrix varies with frequency, then effects of the fibers on the overall electrical properties will be seen in the complex impedance plane.

The present study addresses the microstructure-electrical property relationships of such a composite material, made up of an electrically conductive matrix that contains small amounts of short conductive fibers. In addition to measurements made on actual composites, laboratory simulations involving single wires in dielectric media were carried out to show how the presence of fibers affects the electrical properties in well-controlled situations in which the fiber size and position were precisely known. These laboratory simulations were checked by pixel-based theoretical computations, to verify the phenomena observed and the mechanisms inferred. The results are applicable to relevant conductive fiber/poorly conductive matrix situations, including ceramic, cement/concrete, and polymer matrices. We next briefly review the relevant literature before going on to our new results and frequency-switchable fiber coating model.

2. Previous results

The effect on composite electrical behavior due to the presence of highly conductive fibers is typically discussed with reference to the percolation threshold of the fibers [2, 3]. When enough fibers have been added

* *Present address*: Universitat Politècnica de Catalunya, Department of Electronic Engineering (ETSETB), 08034 Barcelona, Spain.

to the matrix, the fibers are above the percolation threshold, which is defined as a characteristic volume or number fraction of fibers at which continuous paths for electrical current exist in the composite. Some of these paths can occur through parts of the matrix where there has been dielectric breakdown between fiber tips, although most of the conduction is probably through touching fibers. The highly conductive fibers dominate conduction.

Uni-directional continuous fiber-reinforced composites also fall in the "percolating fiber" case. For these materials, the conductivity in the fiber direction should scale with the overall cross-sectional area of the fibers. For a time, this relationship was employed in an ASTM standard for assessing the fiber content of unidirectional fiber-resin composites [4]. It has also been utilized to follow the fracture of unidirectional composites in static or dynamic loading [5–7]. The conductivity exhibits discontinuities as individual fibers break in loading or during fatigue, leading to "self-monitoring" behavior with respect to permanent damage [7].

Below the fiber percolation threshold, interesting transport behavior is also observed in discontinuous fiber composites. Although the matrix dominates the conduction processes, these processes can be strongly influenced by the highly conducting fibers. Rocha and Acrivos [8] developed a model for the thermal conductivity of a dilute suspension of conducting fibers. By "dilute" is meant a low enough volume fraction of fibers so that the presence of one fiber does not influence the effect of nearby fibers. This model was later extended by Frederickson and Shaqfeh [9] into the semi-dilute regime, where certain of the many-body interactions (influence of fibers on each other) were taken into account. Mackaplow *et al*. [10] conducted a numerical study of thermal transport in fiber suspensions, incorporating two-body interactions. These models all predicted that the change in composite conductivity should scale as nL^3, where n is the number density of fibers of length L. This prediction was confirmed by the recent experimental work of Sundararajakumar and Koch [11]. These authors made isotropic fiber suspensions of chopped carbon fibers in a polyalkylene glycol matrix made moderately conductive by the addition of a small amount of KCl. High frequency conductivity measurements (10^4–10^5 Hz) were employed to eliminate the double layer impedance on the fiber/electrolyte surfaces (see Section 3 below), which complicated an earlier DC study [12], thereby allowing true conductive fiber/poorly conductive matrix behavior to be observed.

The most extensive investigation of the electrical behavior of conductive short fiber composites of various kinds has been carried out by Chung and coworkers [7, 13–15]. This work involved three types of matrices—polymer [13], concrete [14, 15], and ceramic [16]. Strain-induced DC resistance changes were attributed to various factors, including partial pull-out of crack-bridging fibers, changes in contact resistance between fiber and matrix, and changes in fiber alignment/spacing (highly oriented systems), with potential for piezoresistive applications [17].

A multi-frequency AC conductivity/impedance approach to the study of conductive short fiber composites is a relatively recent development. Fricke [18] derived the first dispersion equations for the conductivity and permittivity of dilute suspensions of conductive ellipsoids in a less conductive matrix, later translated into complex impedance/modulus plots by Bonanos *et al*. [19]. Two arcs were clearly visible in modulus representation, but not in impedance (Nyquist) representation, most likely due to the absence of polarization/film impedances on the dispersed particles. Han and Choi [20] recently modeled the DC and AC electrical properties of 2-D conductor/insulator composites, obtaining double and even triple arcs in modulus plots, with pronounced fiber orientation effects. Gu *et al*. [21] observed a single bulk impedance arc in fiber-reinforced cement-based composites, using nonconductive wollastonite micro-fibers.

However, all reports involving conductive fiber composites with a less conducting matrix have exhibited two bulk arcs in Nyquist plots, similar to Fig. 1 [22]. In this instance, 1% by weight of short steel fibers was added to hydrating cement paste with a 0.4 water-to-cement ratio (for details, see below). We will refer to this figure when discussing the other results from the literature. As can be seen in Fig. 1, the addition of conducting fibers at this level has an insignificant effect on the DC (low frequency) conductivity. Note that the bulk resistance, R_{DC}, is found at the real axis intersection of the bulk arc(s) and the start of the electrode arc observable on the far right of the diagram. In all impedance plots in this paper, frequency increases from right to left. The presence of conducting fibers clearly subdivides the bulk arc into low frequency and high frequency arcs. We refer to the intersection of the two bulk arcs as R_{CUSP}. The ratio,

$$\gamma = (R_{DC} - R_{CUSP})/R_{DC} \tag{1}$$

or the ratio of the low frequency arc size to the overall DC resistance, is an important parameter for characterizing the complex conductivity of conductive fiber composites. For the random short steel fiber-in-cement paste composite of Fig. 1 this parameter is 0.33. Short carbon fiber cement-based composites have been studied [23] and are also the focus of the present work. Two bulk impedance arcs are typically observed for these composites as well (see below). Gerhardt [24] reported

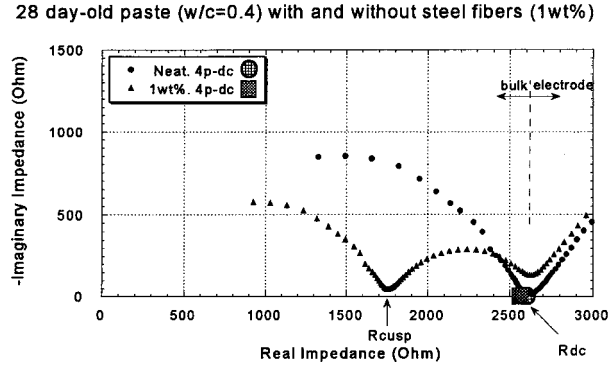

Figure 1 Impedance spectra for a random short steel fiber/cement matrix composite vs. the matrix without fibers, at 28 days of hydration. Note the DC resistance values, obtained by separate 4-point measurements.

Nyquist plots for hot-pressed mullite matrix composites with 10% SiC whiskers. Parallel to the hot-pressing direction (perpendicular to the prevailing whisker orientation) γ was approximately 0.35. It was greater than 0.90 perpendicular to the hot-pressing direction. Nearly uniaxial fiber orientation was achieved by Wang *et al*. [25] in extruded/hot-pressed Si_3N_4 matrix/SiC whisker composites (20 wt% fibers). When measured perpendicular to the fiber axis, γ was essentially zero (a single bulk arc), whereas it was high ($\sim$0.85) in the direction of the fibers.

The preceding examples involved ceramic (cement, oxide, or nitride) matrices. There is evidence that under certain circumstances, polymer matrix composites can exhibit similar two-arc impedance behavior. Kaushik *et al*. [26] studied the degradation of carbon fiber/vinyl ester composites (20 vol% fibers) submerged in concentrated NaCl solution and subjected to electrochemical potential gradients. The single capacitive feature in Nyquist plots of the pristine composite (due to the resistive polymer matrix) gradually evolved into the dual-arc behavior characteristic of chopped conductive fiber composites, with values of γ in excess of 0.9. This was interpreted as being due to slow penetration of the electrolyte into microscopic but percolated pores in the polymer matrix, rendering it moderately conductive.

3. The frequency-switchable fiber coating model

The dual-arc impedance behavior of short conductive fiber composites can be rationalized on the basis of the model pictured in Fig. 2. This model is based on recent work with single and multiple fibers (steel, copper) suspended in a low conductivity medium (tap water) and measured or modeled for impedance response along the axis of the fibers [27]. The unique frequency-dependent behavior arises due to highly resistive "coatings" on the conductive fibers. In the case of steel, these may or may not include a passive oxide film. In all cases, however, a polarization layer (double layer/charge transfer resistance) forms at the fiber: electrolyte interface. Under DC and low frequency AC excitation, these layers act to make the fibers insulating, so that their effect on overall electrical transport through the composite is negligible. In terms of the equivalent circuit in Fig. 2b, the bottom path is open and the current flow (dashed line in Fig. 2a) is unperturbed from the no-fiber situation. As frequency increases, however, the "coating" impedance goes to zero, causing the fibers to act as short-circuits in the composite. The "switch" is closed on the lower path in Fig. 2b, which becomes increasingly important in overall transport. The result is the subdivision of the single Nyquist arc, in the case with no fibers, into two separate arcs. The diameter of the high frequency arc is given by the difference between the resistance of a composite with insulating fibers (low frequency) and the resistance of a composite with highly conducting fibers (intermediate frequency). When the fibers are highly conducting, the composite resistance is a combination of matrix resistance (between fibers and between fibers and the electrodes) and spreading

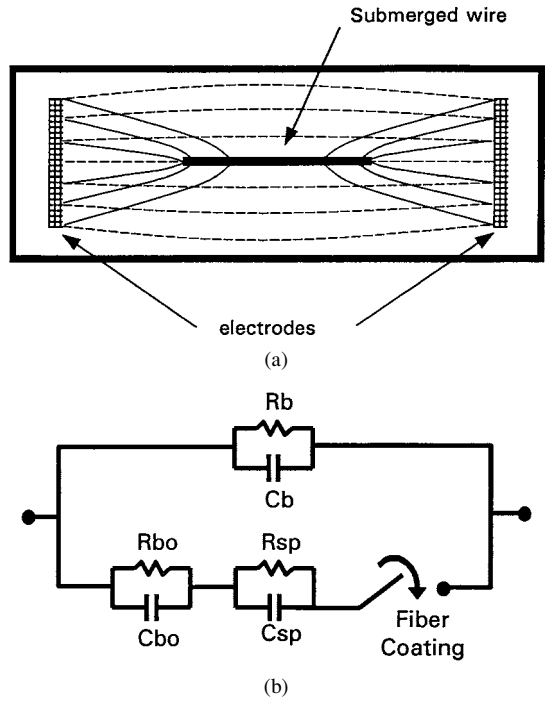

Figure 2 Schematic diagrams of (a) current flow and the (b) equivalent circuit for the frequency-switchable fiber coating model. At DC and low AC frequencies, the fiber "coating" (double layer impedance and/or oxide film) is insulating and the bottom path is "open" in (b); the current flow in (a), the dashed lines, is as if the fiber were not present (R_b, C_b; b = bulk). By intermediate frequencies, however, the coating impedance is eliminated and the "switch" is thrown in the lower path of (b), which now dominates current flow in (a), the solid lines. In the bottom path, "bo" stands for the outer bulk regions, and "sp" stands for the spreading resistance/capacitance associated with the current-bunching (spreading resistance) zones at the fiber tips.

resistance due to current-bunching at the fiber tips (i.e., the solid current lines in Fig. 2a). The current constriction at intermediate frequencies was confirmed by grey-scale images of current density in pixel-based computer calculations [27]. Some amount of current constriction occurs for any shape of highly-conducting inclusion, including spherical inclusions [27], but is greatest for inclusions that are long and thin in the direction of the applied field [1, 27].

Although the basic features of the impedance response of short conductive fiber compsites (relative insensitivity of the DC resistance to the presence of fibers and subdivision of the bulk impedance are into two arcs) have been qualitatively explained, quantitative relationships between experimental parameters such as R_{CUSP} (or γ) and composite microstructure must be developed. The present study investigated the roles of fiber pull-out, fiber debonding, and fiber orientation on the impedance response of conductive fiber composites. As in our prior study [27], a combination of physical simulation (fibers in tap water) and pixel-based computer modeling was employed, to compare and contrast with actual composite behavior.

4. Experimental details

Random short fiber composite: The specimen whose impedance data are displayed in Fig. 1 was prepared from Type I portland cement at a water-to-cement ratio

of 0.4 by weight. Steel fibers (1% by weight, average length 2 mm, diameter 30 μm) were dry-mixed with the cement in a Hobart planetary mixer for 1 min. The water was added, and mixing continued for 3 min at low speed, followed by hand mixing for 1 min, and 3 additional minutes of machine mixing. The specimen was cast in a rectangular polycarbonate container ($25 \times 25 \times 100$ mm) with plain carbon steel (C-1018) electrodes cast in place at a separation of 90 mm. The sample was sealed and stored in a water-saturated environment until impedance measurements were performed.

Oriented short fiber composites: A small-scale ram type extruder was used to produce sheet specimens (25.4 mm wide by 8 mm thick), at a rate of 1.2 mm/min. The overall composition was Type I portland cement with 0.5 vol% carbon fibers (4 mm final length, 8 μm diameter), and 5% silica fume; 0.6% superplasticizer and 0.8% methylcellulose (extrusion aid) were added by weight. The water-to-solids ratio was 0.3. The liquid phase was first mixed with the fibers to distribute them, and then the solid materials were mixed together in a Hobart planetary blender for 10 min. After extrusion, the specimens were cured under a plastic sheet for one day and then cured in 100% RH for 45 days.

Physical simulations: Physical simulations were carried out using polycarbonate containers with plain carbon steel (C-1018) electrodes at the ends, but employing tap water as the electrolyte. Our prior work showed that tap water had the appropriate conductivity to simulate the conductivity of mature cement-based specimens. Furthermore, polarization/film impedances form on the surface of steel wires embedded in the tap water, just like in real composites, resulting in coating impedances that are responsible for the frequency-switchable behavior of conductive fiber composites.

For simulations of fiber pull-out, the apparatus in Fig. 3a was employed. A vertical 50 mm wire (0.5 mm diameter) top electrode was suspended above a graduated cylinder ($\sim 3.8 \times 10^3$ mm^2 cross section) with a copper gauze bottom electrode as shown. The distance between the tip of the wire and the gauze electrode was fixed at 61 mm. Water was added until it just touched the bottom of the tip, and the first impedance measurements were made. Carefully weighed amounts of water were added, from which accurate calculations of the increasing tip submersion were made. Impedance measurements were made as a function of tip submersion. The length of the fiber that was outside the water corresponded to the amount of fiber that would be pulled-out in a mechanical test.

Simulations of fiber debonding were carried out in a polycarbonate cell identical to that employed for the random short fiber composite ($25 \times 25 \times 100$ mm), with 90 mm spacing between the electrodes. A 50 mm long 304 steel wire (0.5 mm diameter), coated with an electrically insulating polymer sheath and sealed at the ends, was suspended on insulating supports along the axis of the cell and equidistant from the electrodes. Impedance measurements with and without the supports (in the absence of the wire) showed that these did not contribute to the impedance spectra obtained. Impedance measurements were made with the horizontal coated wire, and subsequently with progressively larger amounts of insulation stripped from each end (2 mm, 5 mm, etc.). The configuration was similar to that represented by Fig. 2a.

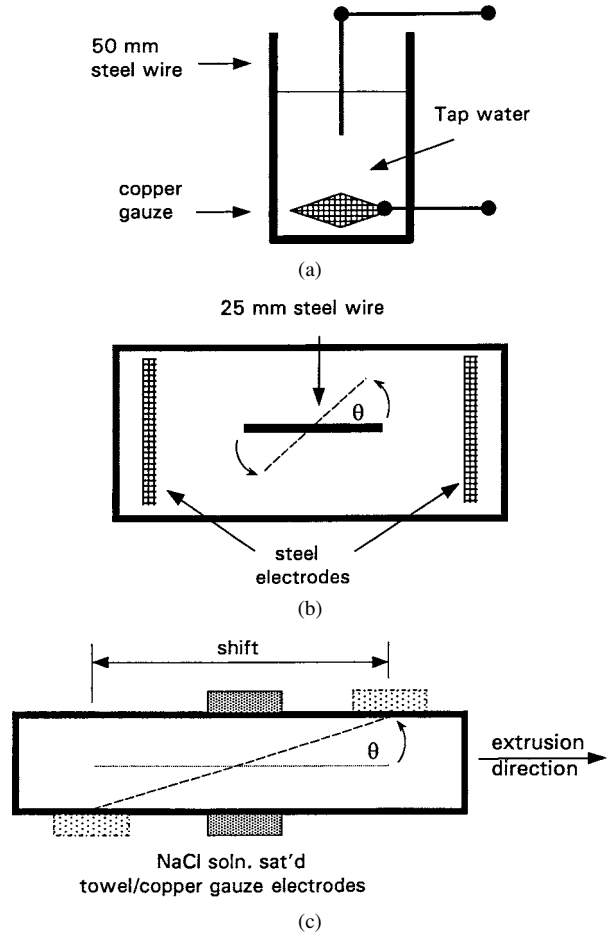

Figure 3 Schematics of (a) the "pull-out" experiments, where the amount of submersion in tap water of a 50 mm long, 0.5 mm diameter, wire was systematically varied, (b) the fiber rotation studies, where a 25 mm long steel wire (0.5 mm diameter) was positioned along the axis of a tap water cell equidistant from two electrodes 31 mm apart, and rotated as shown, and (c) the composite orientation studies, where varying angles of field application relative to the direction of extrusion were accomplished by shift of the opposing electrodes. Impedance measurements were made in (a) between the submerged wire and the copper gauze bottom electrodes as a function of wire submersion, in (b) between the external steel electrodes as a function of rotation angle, θ, and in (c) between opposing copper electrodes as they were shifted in opposite directions as shown.

Fiber orientation studies were made in a shortened polycarbonate cell ($25 \times 25 \times 31$ mm), with a 25 mm bare 304 steel wire (0.5 mm diameter), as shown in Fig. 3b. The shortened cell was used to make it easier to see the fiber arc at large angles between the applied field and the wire, by increasing the value of γ (or $(R_{DC} - R_{CUSP})/R_{DC}$) via minimizing the size of the high frequency arc (the wire-to-electrode contribution). Sufficient distance was maintained between the wire tips and the electrodes in the $\theta = 0$ configuration (3 mm) in order to avoid end effects. In these studies, impedance spectra were taken as a function of the orientation angle between the wire and the direction of the applied field.

Fiber-orientation measurements were also made on an extruded carbon fiber specimen using the electroding

scheme in Fig. 3c. Copper gauze electrodes 6 mm wide and running the width of the specimen were in contact with paper towel strips of the same dimension, which in turn were in contact with the surface of the sample. The paper towel strips were saturated with NaCl solution, to facilitate electrochemical contact with the sample. By shifting the centerlines of the top and bottom electrodes in opposite directions, the angle between the prevailing fiber direction and the direction of applied field was systematically varied, as shown.

Impedance measurements: Impedance studies were carried out using a personal computer-controlled frequency response analyzer (Solartron 1260 with Z60 control software, Schlumberger, Cambridge, UK)† over the frequency range of 0.1 Hz to 10 MHz (10 points per decade). The excitation amplitude was varied from 25 mV to 1.0 V, with no obvious change in bulk spectral features. The spectra were analyzed using the "Equivalent Circuit"† software package [28].

The largest source of error in impedance measurements involves uncertainty in inter-electrode spacing, which is estimated to be ±5%. For a given series of tests, however, the spacing was maintained so as to further minimize uncertainty. In the physical simulations, the conductivity of the tap water can be quite sensitive to extraneous minerals introduced by handling. To confirm that the water had not changed conductivity as a result of testing, its conductivity was measured before and after each series of tests.

Numerical simulations: Two FORTRAN 77 numerical programs, **ac3d.f** and **elecfem3d.f**, were used to carry out pixel-based computer calculations. These programs can be accessed at http://ciks.cbt.nist.gov/garboczi/, Chapter 2, along with a manual in HTML or hard copy format [29]. These programs were designed to compute the electrical properties of random materials whose microstructure can be represented by a 3-D digital image. They can also be used to simulate non-random, but analytically intractable geometries, as in the present study. The program **ac3d.f** is a finite difference program, for finite frequencies, and was used for all the frequency-dependent computations described in this paper. The program **elecfem3d.f** is a finite element program, for use in DC problems only. It was used for computations of the fiber pull-out laboratory simulation described above.

Pixels in a 3-D digital image were used to construct representations of each laboratory simulation studied (fiber pull-out, fiber debonding, and fiber orientation). The length scale generally used was 0.5 mm/pixel and the number of pixels used matched the overall sample dimensions. For example, the fiber orientation studies employed a system of $62 \times 62 \times 62$ pixels, closely matching the $25 \times 25 \times 31$ mm sample. The electrode-to-electrode dimension, 31 mm, was the most important dimension to match exactly, as these were close to the fiber tips. The wires were one pixel or 0.5 mm in width, and were suspended in the middle of the sample chamber as in the experimental arrangement. The debonding computations used a $51 \times 51 \times 182$ pixel cell, and a one pixel wire, closely matching the physical size of the experimental cell used. For the pull-out computation, a length scale of 0.1 mm/pixel was used in the finite element program, in a $137 \times 137 \times 400$ pixel system. The size of the computational system, 13.7 mm × 13.7 mm × 40 mm did not, therefore, exactly match the laboratory set-up. However, the size of the cell used, compared to the wire, was large enough, in both laboratory and computational situations, so that the system size should not have significantly affected the final results.

For the orientation and debonding computations, a finite difference node was placed in the middle of each pixel. Bonds were assigned between each pair of nodes, reflecting the conductivities of the materials around each pair of nodes. Both the electrodes and the wire were taken to be highly conductive. No polarization layer was used on the electrodes, so that the electrode arc was not included or computed. A polarization layer was taken on the surface of the wires, however. The admittance of this layer was taken to be that of comparable electrodes (fitted from experimental impedance data), but adjusted for the differences in the size and shape between the wires and the electrodes. In this way, only the time constant (resistance times capacitance) was specified, so that the unknown conductivity, dielectric constant, and thickness of the layer did not need to be individually determined. The water pixels had the correct admittance for the tap water used (~0.03 S/m). The wire was given a bulk DC conductivity approximately 10^4 times that of the tap water. (The true value would be much larger, but this value was adequate for the computations, which become intractable at much larger values.) Once the model geometry and admittances were set up, a uniform electric field was applied, along the wire in the debonding experiments and at the appropriate angle (θ) to the wire direction for the orientation experiments. For the latter, it was easier to rotate the applied field than to rotate the wire. The frequency was systematically varied, similar to experiment, and the Nyquist plot determined.

In the pull-out computation, the water and air pixels were assigned appropriate conductivities, while the wire, one pixel in width, was assigned a conductivity 1000 times that of the water. There were no coating impedances, as comparison was to be made to the measured value of impedance at a frequency where the wire was highly conducting.

5. Results and discussion

Fiber "pull-out" simulations: Typical impedance curves for the single steel wire at various depths of submersion in tap water are shown in Fig. 4a. (Note that there is only a single bulk arc, due to the fact that the wire is essentially a part of the electrode to which it is attached.) Dramatic changes are seen in the first few mm of submersion; thereafter the changes are more gradual. This is better depicted in Fig. 4b, where we

† Certain commercial equipment is identified in this paper in order to adequately specify the experimental procedure. In no case does such identification imply recommendation or endorsement by the National Institute of Standards and Technology, nor does it imply that the equipment used is necessarily the best available for the purpose.

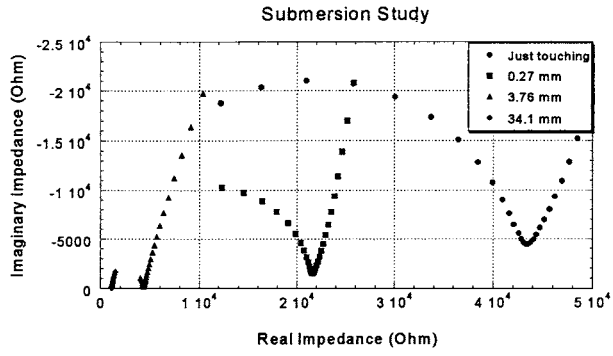

(a)

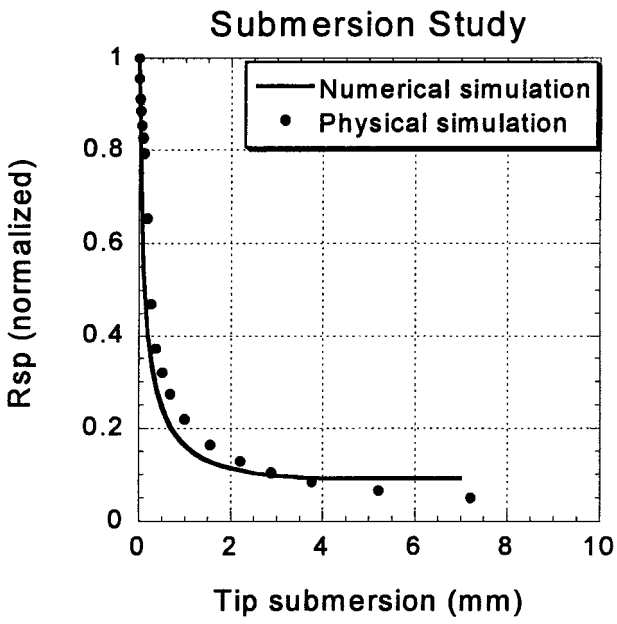

(b)

Figure 4 Results of the pull out/water submersion study corresponding to the cell in Fig. 3a. (a) impedance spectra, and (b) spreading resistance values (cusp values minus the known water resistance for the 61 mm water height). Pull-out can be viewed as the complement of submersion.

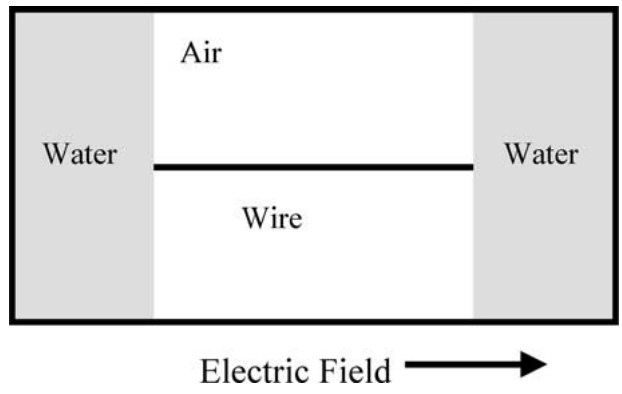

(a)

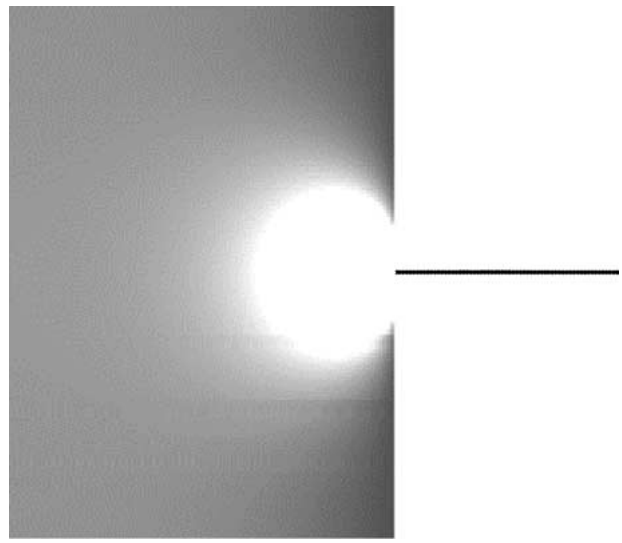

(b)

Figure 5 Showing (a) a schematic of the numerical cell used in the finite element simulation of the pull-out experiement, and (b) a gray scale image of the current density (current increases with lightness of gray scale) when the wire tip was just touching the water surface.

take the resistance at electrode/bulk intercept in Fig. 4a and subtract the resistance, approximately 600 Ω, of the volume of water between the fixed wire tip and the bottom copper gauze electrode. The experimental (circles) and model (solid line) results have both been normalized by their respective values at the point where the wire just touched the water surface. Both experiment and modeling results fall by as much as 90% in the first 3 mm of submersion. Both sets of data are in good qualitative agreement with each other, although there are some quantitative differences. These differences are probably due to the fact that the depth of immersion was hard to measure for the experiment for small immersions (<0.2 mm), because the diameter of the computational cell was about five times smaller than that of the experimental set-up, and because the one-pixel thick wire in the finite element computations did not precisely simulate the cylindrical wire used in the experiment.

Figure 5a shows a schematic view of the computational cell used. A replica was made of double the real system, giving a symmetric system upon which it was much easier to perform numerical computations. Once the overall resistance was computed, the resistance of the part of the wire extending between the water layers was subtracted, and the remaining resistance was divided by two, to give an equivalent resistance to that measured in experiment. A resolution of 0.1 mm/pixel was used, in order to be able to see the behavior of the impedance in the first few tenths of a millimeter immersion of the wire tip, where most of the resistance drop took place.

The results shown in Fig. 4b are a consequence of the "spreading resistance" effect at the wire tip. The spreading resistance of a solid in point contact with an infinitely conducting cylindrical electrode was first established by Holm [30] and placed on a firm mathematical footing by Newman [31]. For a planar point contact the spreading resistance (R_{sp}) is:

$$R_{sp} = (4\sigma a)^{-1} \tag{2}$$

where a is the radius of the cylindrical electrode and σ is the conductivity of the medium being contacted. Based upon the water conductivity and the radius of the wire in the present study, this value should be 33.3 kΩ, to be compared with the "just touching" experimental value of 44.5 kΩ (normalized to unity in Fig. 4b). This disagreement was probably due to the fact that the rate of

change of resistance was extremely large in the first mm of submersion, which is precisely where the amount of submersion is difficult to gauge due to meniscus formation, thereby leading to fairly large experimental uncertainties in this region. After the wire has been submerged a few tenths of a millimeter, better accuracy is obtained for the amount of submersion, so that a better comparison with theory is with the predicted spreading resistance of an embedded hemispherical cap of radius, r [30]:

$$R_{sp} = (2\pi\sigma r)^{-1} \tag{3}$$

which would correspond to a value of 21.2 kΩ. The experimental value at 0.26 mm of submersion, or approximately the same as the wire radius, was 20.9 kΩ. Figure 5b shows a current map of the model results when the wire just touched the water surface, in which the lighter the gray scale, the higher the local current. Dramatic current concentration is seen in this figure near the wire tip.

The results of the submersion experiment can be interpreted in terms of how a crack-bridging conductive fiber might contribute to overall composite conductivity. At DC or low AC frequencies, there is no electrical continuity across the crack because of the insulating surface impedance. At intermediate frequencies, however, this "coating" impedance (polarization or film impedance) becomes negligible, and the fiber then provides electrical continuity across the crack. Increasing fiber pull-out corresponds to decreasing submersion; maximum submersion means minimum pull-out. The flat parts of Fig. 4b show that there is little change in electrical continuity until most of the fiber has been pulled out of the matrix, assuming of course that the part of the fiber still in physical contact with the matrix also maintains electrical contact with the matrix as it is being pulled out.

Fu and Chung [32] attempted to measure the conductivity between a single stainless steel fiber partially embedded in a cement body and external electrodes on that body during debonding and pull-out. Unfortunately, the contact resistance became immeasurably large beyond the maximum shear stress, i.e., during the actual pull-out process. It is conceivable that there was no longer any electrical contact between the fiber and the matrix beyond this point, as proposed by Fu and Chung [32]. However, since only DC measurements were performed, their resistances were probably dominated by the resistance of the passive oxide film on the steel surface. This is known to be quite large, especially so for stainless steel [33]. Based on the present work, we would suspect that physical contact was always maintained, while electrical contact was not seen due to the insulating film impedance on the surface of the fiber. The present work suggests that such work needs to be repeated at frequencies sufficient to overcome this interfacial impedance.

Fiber debonding simulations: The results of impedance studies of a single 50 mm long wire (insulated, 0.5 mm diameter) suspended equidistant from the electrodes (90 mm apart) on the axis of a 25 × 25 ×

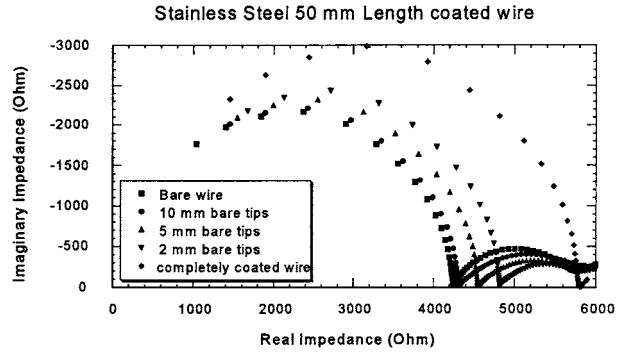

(a)

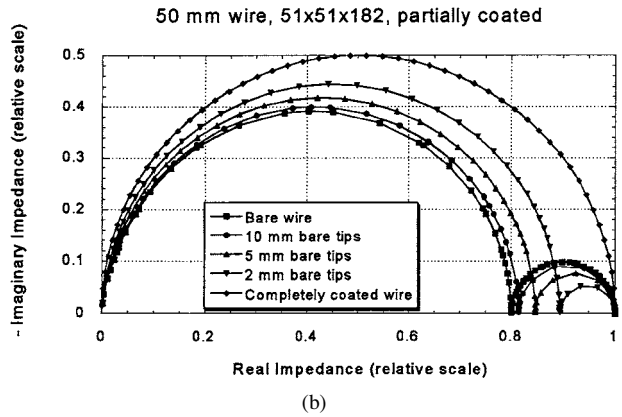

(b)

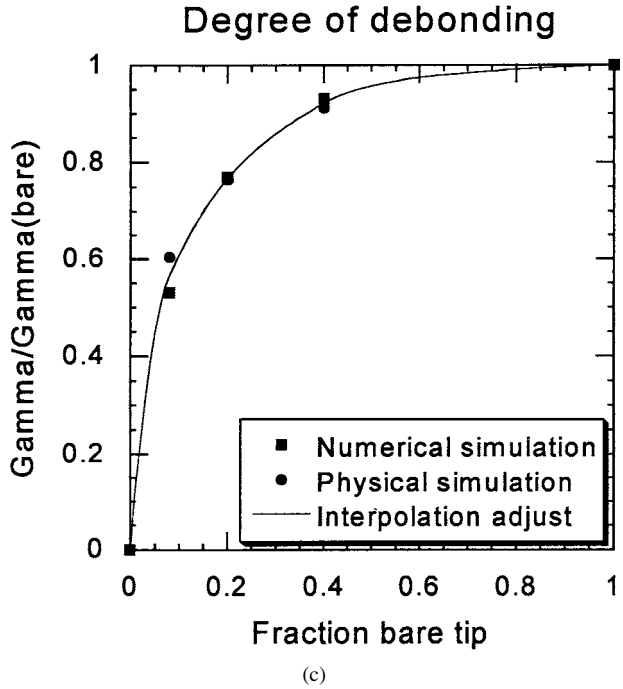

(c)

Figure 6 Results of the debonding/tip exposure study corresponding to the configuration in Fig. 2a. (a) experimental impedance spectra vs. extent of wire tip exposure, (b) computed spectra vs. extent of wire tip exposure, and (c) normalized plot of γ for a bare wire. Debonding can be viewed as the reverse of tip exposure.

100 mm tap water cell are shown in Fig. 6a. The completely coated wire exhibits a single bulk arc, virtually indistinguishable from the cell without the wire, as expected (due to the insulation). As the first 2 mm of insulation is stripped from the ends of the wire, dual arc behavior is obtained. As progressively larger amounts of the ends are exposed, the value of $(R_{DC} - R_{CUSP})$ or γ increases to its maximum value for the bare wire.

Numerical simulations (Fig. 6b) are in excellent agreement with the experimental spectra. If we compute the value of γ at a given degree of tip exposure, and normalize it by the maximum value of γ, obtained for the bare wire, and plot this ratio vs. the degree of tip exposure, the plot in Fig. 6c is obtained. Again, the modeling data points agree well with the experimental data points. The solid line is a spline fit to both sets of data. It is interesting to note that more than 80% of the ultimate change in R_{CUSP} (or γ) occurs within the first 20% of tip exposure.

One can think of tip exposure as the reverse of debonding, assuming of course that debonding means the loss of electrical contact between the fiber and the matrix sheath surrounding it, which may *not* be the case. In the present work debonding is simulated by the presence of increasing lengths of impermeable polymer coating on the middle of the wire. The fraction of the wire covered with polymer is equivalent to the fraction debonded in a debonding situation. Similar to the pull-out situation above, debonding proceeds from right to left in Fig. 6c, from the bare wire (100% electrical contact) to the fully coated wire (no electrical contact). These results suggest that in the early stages of debonding, assuming debonding is equivalent to loss of electrical contact, changes in R_{CUSP} (and γ) will be minor. Only when the fiber is debonded more that about 40% will major changes in composite conductivity take place.

It should be stressed that these changes should be measured at the bulk cusp frequency. The only work to date on single-fiber debonding was the DC resistance study of Fu and Chung [32], mentioned previously. For untreated and acetone-treated steel fibers the contact resistance was high and there were no detectable changes up to the maximum pull-out stress. For acid-treated fibers, however, the contact resistance was significantly smaller and there was approximately an order of magnitude increase in contact resistace up to the maximum stress, beyond which contact was suddenly lost. These results are consistent with progressive debonding taking place along the fiber. By repeating such studies at the bulk cusp frequency in Fig. 6a, it should be possible to eliminate surface impedances and isolate fiber-matrix continuity effects, during both debonding and subsequent pull-out.

Fiber orientation studies: The experimental and computed spectra vs. wire orientation angle are displayed in Figs. 7a and b, respectively. Note that only the low frequency arc is shown for the numerical computations. In both instances, the wire was 25 mm long (0.5 mm diameter) on the axis of a tap-water cell of cross-section 25 mm $\times$ 25 mm and equidistant from the measurement electrodes placed 31 mm apart. The angle, θ, is between the wire and the direction of the applied field. When the wire is perpendicular to the field ($\theta = 90^\circ$), there is no low frequency arc, and the single "bulk" arc is indistinguishable from that of the tap water alone. As θ decreases to zero, where the wire is parallel to the applied field, the maximum value of ($R_{DC} - R_{CUSP}$) or γ is obtained. In Fig. 7c the ratio $\gamma(\theta)/\gamma(\theta = 90^\circ)$ is plotted vs. angle. There is excellent agreement between numerical and experimental results.

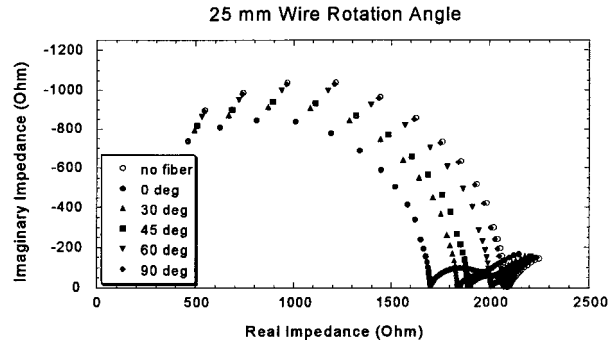

(a)

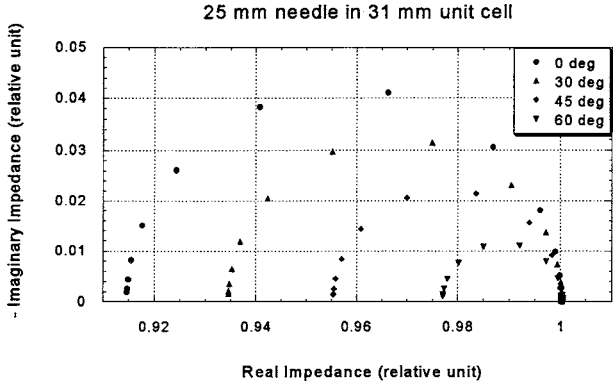

(b)

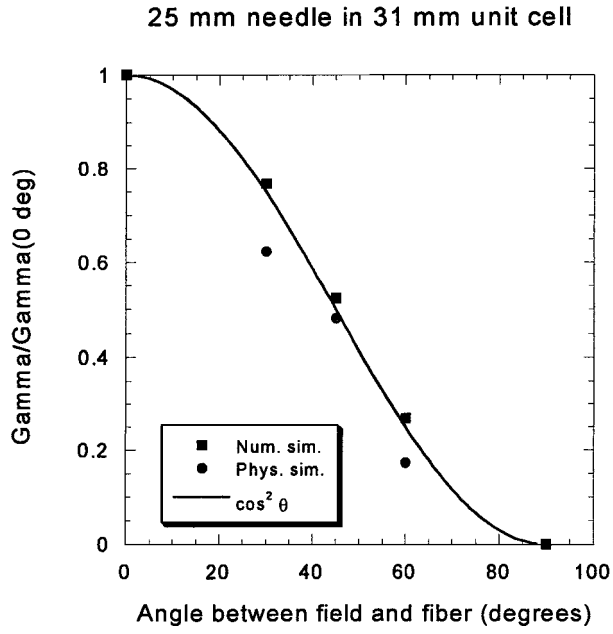

(c)

Figure 7 Result of the wire rotation study corresponding to the cell in Fig. 3b. (a) experimental impedance spectra vs. angle, (b) computed spectra vs. angle, and (c) the $\cos^2\theta$ dependence of the ratio of $\gamma(\theta)$ to $\gamma(\theta = 90^\circ)$.

Also plotted in Fig. 7c is the function, $\cos^2\theta$. This relationship is readily derived by considering the symmetries of the problem. Take the z-axis along the wire direction, and the applied field in the y–z plane with an angle θ between the field and the wire direction, $\vec{E} = E_o\ (0, \sin(\theta), \cos(\theta))$. Using these axes, the combination of matrix plus wire has rotational symmetry around the z-azis, and, since the wire is centered in the

sample cell, it also has a mirror plane (the x–y plane at the wire center) with respect to the z-axis. Therefore, the overall conductivity tensor of the system has the form:

$$\begin{bmatrix} \sigma_{xx} & 0 & 0 \\ 0 & \sigma_{yy} & 0 \\ 0 & 0 & \sigma_{zz} \end{bmatrix} \quad (4)$$

At low frequency, these three components are all comparable and approximately equal to the matrix conductivity. At intermediate frequency, when R_{CUSP} is observed, the xx and yy tensor components are little changed, but now the zz component is much larger. The current resulting from the conductivity tensor in Equation (4) is $\vec{j} = \vec{\vec{\sigma}} \cdot \vec{E}$. In the experimental set-up, the current along the direction of the applied field is measured, or $\vec{j} \cdot \vec{E} = \sigma_{yy} \sin^2\theta + \sigma_{zz} \cos^2\theta$ (normalized by E_o^2). Since σ_{yy} does not change very much with frequency (perpendicular to wire), while σ_{zz} increases greatly with frequency (parallel to wire), the size of the arc should be proportional to $\cos^2(\theta)$, as seen in Fig. 7c.

The most important result of these simulations is that oriented short conducting fiber composites will exhibit the maximum value of γ (or relative size of the low frequency arc) when measured in the direction of the fibers. In a perfectly oriented composite, there should be no measurable low frequency arc ($\gamma = 0$) when measured perpendicular to the fiber direction.

Composite Studies: We are now in a position to interpret the behavior of actual short conductive fiber composites. The impedance spectrum in Fig. 1 is for a 28-day old random steel fiber/cement-matrix composite. The bulk arc subdivision is given by $\gamma \sim 0.33$. In contrast, Fig. 8 displays impedance spectra for a 46 day old extruded carbon fiber/cement matrix composite. The electrode arcs are not shown in Fig. 8. Furthermore, the data have been normalized by R_{DC} in each case, which are listed in the figure caption. The $\theta = 90$ (zero shift) behavior is similar to Fig. 1, with $\gamma = 0.4$. The fact that it is not zero (compare with Fig. 7) is due to the fact that the orientation in the plane of the sample is not perfect. On the other hand, as θ is decreased, γ increases to a value of 0.8 at $\theta \sim 18^\circ$ (24 mm shift) consistent with the trend in Fig. 7c and also with prior observations [24–26], i.e., that subdivision of the bulk arc in highly oriented composites is small (or even zero) when measured perpendicular to the fiber direction, and maximum (approaching 100%) in the plane (or direction) of the fibers.

It should be stressed that other factors (number density of fibers, fiber aspect ratio, distribution of fiber lengths, distribution of fiber orientations, etc.) will also play a role in determining bulk arc subdivision, just as they do in determining the percolation threshold. For example, the fiber content (number density) was much higher in the studies cited in the Introduction [24–26], undoubtedly contributing to the higher values of γ. Furthermore, Gerhardt [24] and Wang *et al.* [25] reported large decreases in the DC resistance when measuring parallel vs. perpendicular to the fiber direction. Even after correcting for changes in geometry, the DC conductivity is clearly being altered to a large extent by the presence of the fibers. Below the percolation threshold, we predict there should be only minor changes in DC conductivity due to fibers, assuming that the fibers are insulated by their interfacial impedances. What these results suggest is that there must be a high degree of fiber–fiber contact in the direction of preferred orientation, albeit not yet fully percolating. The aspects of fiber number density, fiber aspect ratio, distribution of fiber lengths and orientation, etc., are the subjects of ongoing research.

General discussion: The necessary conditions for the unique impedance behavior of short conductive fiber composites documented in the present study are:

- *Highly conductive fibers*: Insulating fibers may play a role in controlling matrix cracking [21], but will not contribute directly to composite conduction, whether in DC or AC measurements.
- *A finitely conductive matrix*: Below percolation, a composite made with an insulating matrix will also be insulating. The degradation of carbon fiber/vinyl ester composites (insulating in their pristine condition) when submerged in concentrated NaCl solution and subjected to electrochemical potential gradients [26] converted an otherwise insulating matrix into a marginally conductive electrolyte, enabling frequency-switchable composite behavior as in the present study. The mullite matrix in SiC whisker/mullite composites [24] is not known to be conductive at room temperature, but grain boundary effects may play a role.
- *A frequency-switchable surface impedance on the fibers*: For good electronic conductors (carbon, steel) in an electrolyte matrix (cement, polymer electrolyte), this derives from the double layer/polarization resistance. In addition, a highly resistive passive oxide film forms on iron or steel in the high pH pore solution of cement-based matrices. The origin of the surface impedance for SiC whiskers in ceramic matrices (mullite, Si_3N_4) is an open question. One possibility, common in the field of electroceramics, is the formation of space charge layers at the interfaces between dissimilar

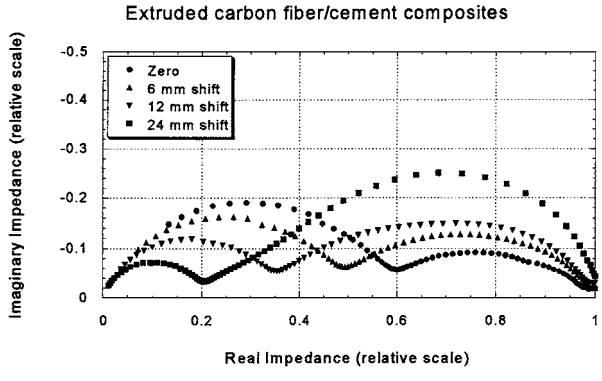

Figure 8 Experimental impedance spectra vs. orientation angle (shift of electrodes in Fig. 3c) for an extruded carbon fiber composite (0.5 vol% fibers). Electrode arcs are omitted and the data have been normalized by the DC resistance in each case—zero shift (1.9 kΩ), 6 mm shift (3.7 kΩ), 12 mm shift (8.2 kΩ), and 24 mm shift (27 kΩ).

semiconductors. Such space charge layers are known to exhibit frequency-switchable impedance behavior [34].

6. Conclusions

Short conductive fiber composites, below their percolation threshold, can exhibit dual arc impedance behavior. The subdivision of the bulk arc is attributable to a frequency-switchable surface impedance on the fibers. This impedance renders the fibers insulating at DC and low AC frequencies. At intermediate frequencies, however, the surface impedance disappears and the fibers act as microstructural short circuits. The residual resistance is a combination of inter-fiber regions and spreading resistance zones near the fiber tips.

Physical simulations (wires in tap water cells) combined with pixel-based numerical computations have demonstrated how several factors—fiber pull-out, fiber/matrix debonding, and fiber orientation—can influence the fiber-induced bulk arc subdivision. This can be quantified by the parameter γ, defined as the ratio of the high frequency arc width to the overall DC resistance. The γ parameter can be quite large for a fully submerged (intact), bare (fully bonded) fiber aligned in the direction of the applied field, meaning that the fiber greatly reduces the composite resistance at intermediate frequencies. However, the γ parameter is relatively unaffected by pull-out or debonding of the fiber until the final stages of either process. In contrast, the bulk arc subdivision is significantly influenced by the fiber orientation with respect to the electric field direction. The γ parameter is largest when measured in the fiber direction, and least (or zero) when measured perpendicular to it. These results explain, at least qualitatively, the orientation dependence of impedance measurements on highly oriented short conductive fiber composites.

It is clear that in the case of highly conducting fibers in a poorly conducting matrix, where the fibers have a frequency-switchable coating impedance, many of the fiber aspects that are important in mechanical behavior, like fiber pull-out, fiber debonding, and fiber orientation, can be quantitatively observed with impedance spectroscopy. Since impedance spectroscopy is a nondestructive technique, these results open the door for non-invasive monitoring of the mechanical state of composites, which are mechanically dominated by the presence of fibers.

Acknowledgments

This work was supported by the National Science Foundation Science and Technology Center for Advanced Cement-Based Materials under grant no. CHE-91-20002. JMT acknowledges the support of the Spanish Government through Secretary of the State for Universities, Research and Development of the Ministry of Education and Culture under grant no. PR98-0036975531.

References

1. J. F. DOUGLAS and E. J. GARBOCZI, *Adv. Chem. Phys.* **91** (1995) 85.
2. R. ZALLEN, "The Physics of Amorphous Solids" (Wiley, New York, 1983) pp. 135–204.
3. D. S. MCLACHLAN, M. BLASZKIEWICZ and R. E. NEWHAM, *J. Am. Ceram. Soc.* **73** (1990) 2187.
4. Test Method for Fiber Content of Unidirectional Fiber-Resin Composites by Electrical Resistivity, ASTM D 790-84a (1980), discontinued in 1988.
5. N. MUTO, H. YANAGIDA, T. NAKATSUJI, M. SUGITA and Y. OHTSUKA, *J. Am. Ceram. Soc.* **76** (1993) 875.
6. X. WANG and D. D. L. CHUNG, *Smart Mater. Struc.* **6** (1997) 504.
7. D. D. L. CHUNG, *Mat. Sci. Eng.* **R 22** (1998) 57.
8. A. ROCHA and A. ACRIVOS, *Q. J. Mech. Appl. Math.* **26** (1973) 441.
9. G. H. FREDRICKSON and E. S. G. SHAQFEH, *Phys. Fluids* **A 1** (1989) 3.
10. M. B. MACKAPLOW, E. S. G. SHAQFEH, and R. L. SHIEK, *Proc. Royal. Soc. Lond.* **A 447** (1994) 77.
11. R. R. SUNDARARAJAKUMAR and D. L. KOCH, *ibid.* **A 455** (1999) 1923.
12. A. ROCHA and A. ACRIVOS, *ibid.* **A 337** (1974) 123.
13. X. WANG and D. D. L. CHUNG, *Sensors and Actuators* **A 71** (1998) 208.
14. P.-W. CHEN and D. D. L. CHUNG, *J. Am. Ceram. Soc.* **78** (1995) 816.
15. *Idem.*, *ACI Mat. J.* **93** (1996) 341.
16. S. WANG and D. D. L. CHUNG, *Smart Mater. Struc.* **6** (1997) 199.
17. X. WANG and D. D. CHUNG, *Carbon* **35** (1997) 1649.
18. H. FRICKE, *J. Phys. Chem.* **57** (1953) 934.
19. N. BONANOS, B. C. H. STEELE, E. P. BUTLER, W. B. JOHNSON, W. L. WORRELL, D. D. MACDONALD and M. C. H. MCKUBRE, in "Impedance Spectroscopy: Emphasizing Solid Materials and Systems," edited by J. R. Macdonald (Wiley, New York, 1987) p. 191.
20. D. G. HAN and G. M. CHOI, *Electrochim. Acta* **44** (1999) 4145.
21. P. GU, Z. XU, P. XIE and J. J. BEAUDOIN, *Cem. Concr. Res.* **23** (1993) 675.
22. S. J. FORD, J. D. SHANE and T. O. MASON, *ibid.* **28** (1998) 1737.
23. X. FU, E. MA., D. D. L. CHUNG and W. A. ANDERSON, *Cem. Concr. Res.* **27** (1997) 845.
24. R. GERHARDT, *Proc. Cer. Eng. Sci.* **15** (1994) 1174.
25. C.-A. WANG, Y. HUANG, Y. LI and Z. ZHANG, *J. Am. Ceram. Soc.* **83** (2000) 2689.
26. D. KAUSHIK, M. N. ALIAS and R. BROWN, *Corrosion* **47** (1991) 859.
27. J. M. TORRENTS, T. O. MASON and E. J. GARBOCZI, *Cem. Concr. Res.* **30** (2000) 585.
28. B. A. BOUKAMP, "Equivalent Circuit (EQUIVCRT.PAS)," Dept. of Chemical Engineering, University of Twente, The Netherlands (1990).
29. E. J. GARBOCZI, "Finite element and finite difference programs for computing the linear electric and elastic properties of digital images of random materials," NIST Internal Report 6269 (1998). Also available at http://ciks.cbt.nist.gov/garboczi/, Chap. 2.
30. R. HOLM, Electric Contacts: Theory and Application" (Springer-Verlag, New York, 1967).
31. J. NEWMAN, *J. Electrochem. Soc.* **113** (1966) 501.
32. X. FU and D. D. L. CHUNG, *ACI Mater. J.* **94** (1997) 203.
33. S. J. FORD and T. O. MASON, in "Techniques to Assess the Corrosion Activity of Steel Reinforced Concrete Structures," edited by N. S. Burke, E. Escalante, C. K. Nmai and David Whiting, ASTM STP 1276 (1995).
34. D. S. MCLACHLAN, J.-H. HWANG and T. O. MASON, *J. Electroceramics* **5** (2000) 37.

Received 3 November 1999
and accepted 13 July 2000